Stimulation of Electro-oxidation Catalysis by Bulk-structural Transformation in Intermetallic $ZrPt_3$ Nanoparticles

Gubbala V. Ramesh,[*,†] Rajesh Kodiyath,[†] Toyokazu Tanabe,[†] Maidhily Manikandan,[†,§§§] Takeshi Fujita,[§,⊥] Naoto Umezawa,[†,⊥] Shigenori Ueda,[§§] Shinsuke Ishihara,[‖,⊥] Katsuhiko Ariga[‖,⊥] and Hideki Abe[*,†,⊥]

† National Institute for Materials Science, 1-1 Namiki, Tsukuba, Ibaraki 305-0044, Japan

§§§ Crystal Growth Centre, Anna University, Chennai, Tamil Nadu 600-025, India

⊥ Precursory Research for Embryonic Science and Technology (PRESTO) and Core Research for Evolutional Science and Technology (CREST), Japan Science and Technology Agency (JST), 4-1-8 Honcho, Kawaguchi, Saitama 332-0012, Japan

§ WPI Advanced Institute for Materials Research, Tohoku University, Sendai 980-8577, Japan

§§ Synchrotron X-ray Station at SPring-8, National Institute for Materials Science, 1-1-1 Kouto, Sayo, Hyogo 679-5148, Japan

‖ WPI International Center for Material Nanoarchitectonics, National Institute for Materials Science, 1-1 Namiki, Tsukuba, Ibaraki 305-0044, Japan

Corresponding Authors:

GUBBALA.Venkataramesh@nims.go.jp
ABE.Hideki@nims.go.jp

Supporting Information

1 *p*XRD

2 HX-PES

3STEM/TEM

4 Electrochemistry

1. *p*XRD

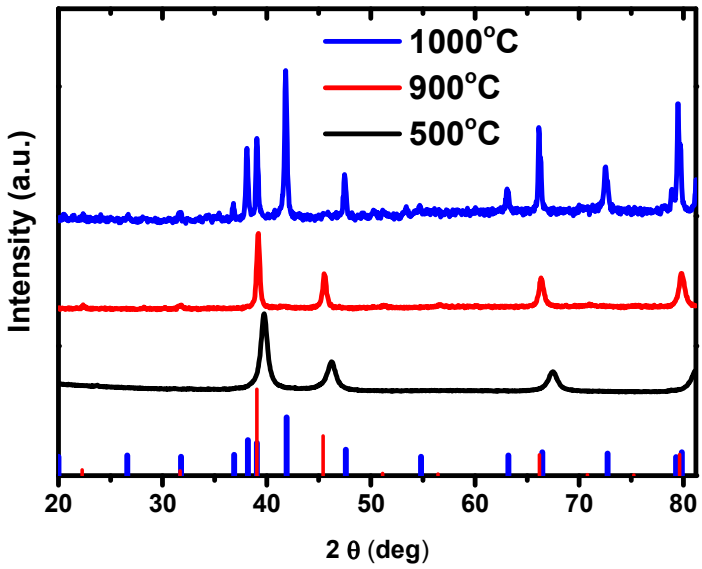

Figure S1. *p*XRD profiles of the Zr-Pt NPs annealed at different temperatures. A simulated *p*XRD pattern for the ordered cubic (red) and hexagonal (blue) $ZrPt_3$ intermetallic phase is shown at the bottom.

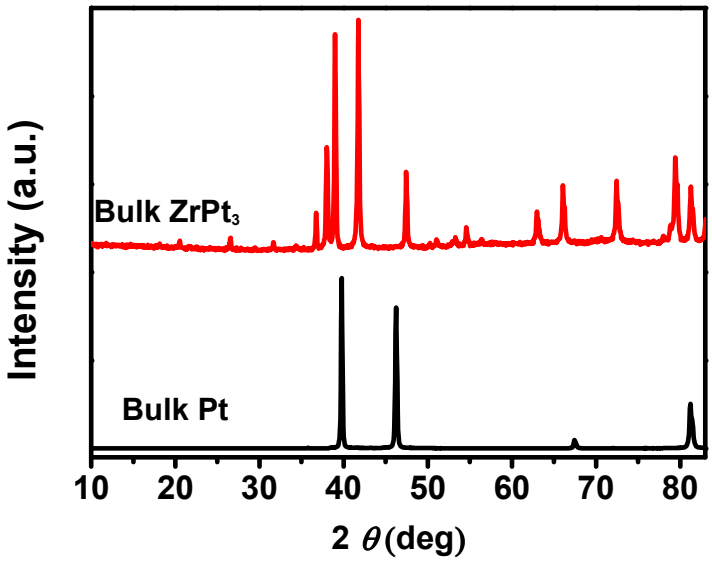

Figure S2. *p*XRD profiles of bulk $ZrPt_3$ and bulk Pt.

2 HX-PES

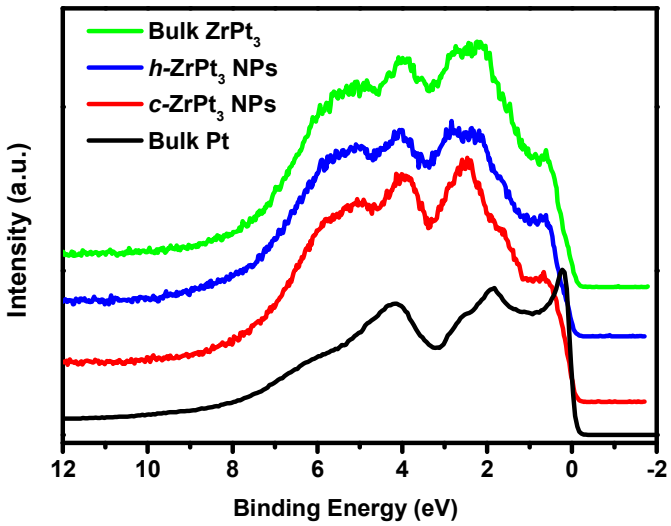

Figure S3. HX-PES spectra in the valence *d*-band region for the *c*-$ZrPt_3$ NPs and *h*-Zr-Pt alloy NPs. The HX-PES spectra for bulk Pt and $ZrPt_3$ are shown as the reference.

3 STEM/TEM

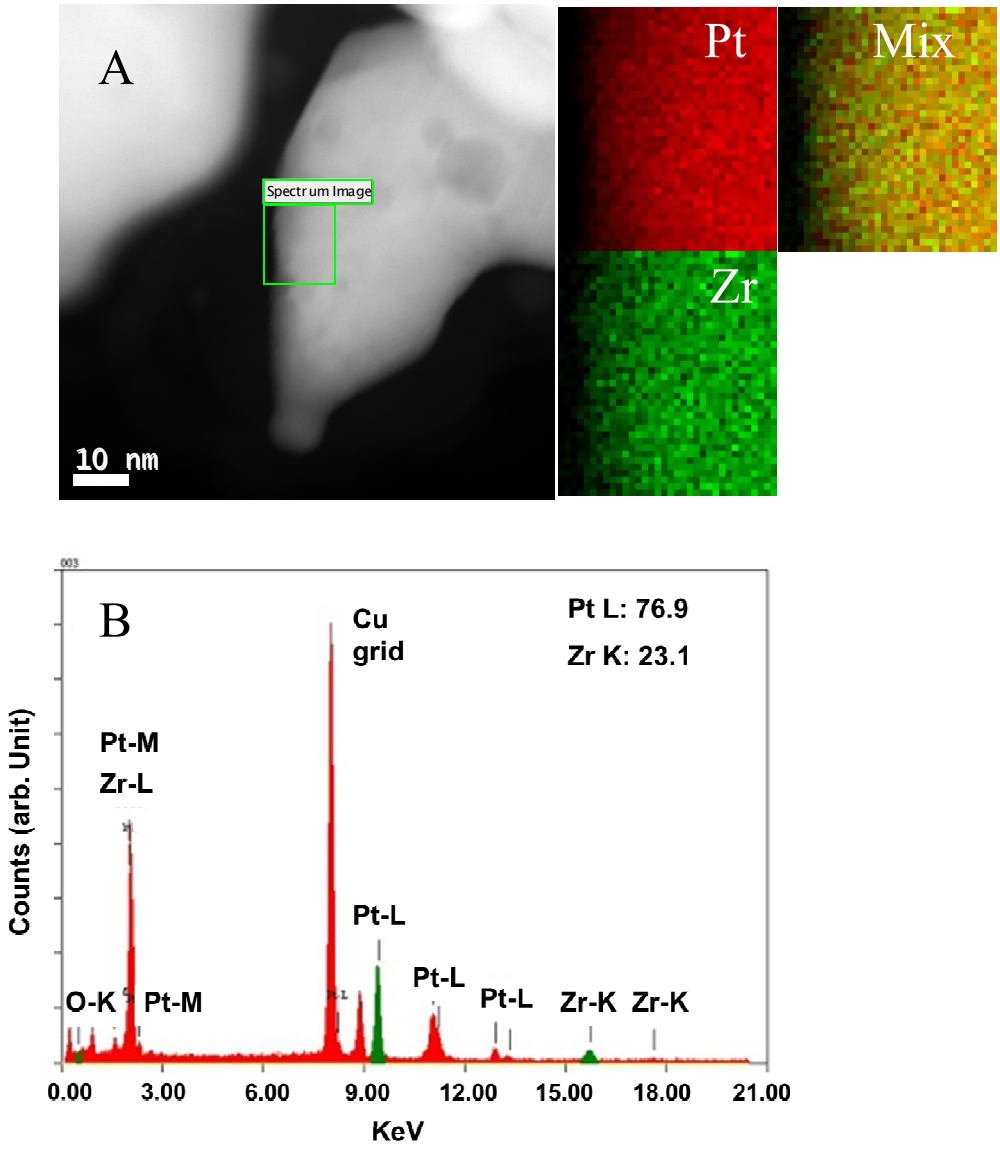

Figure S4. A) STEM image of *c*-$ZrPt_3$ NPs and the corresponding compositional-mapping images. B) The result of compositional analysis is presented.

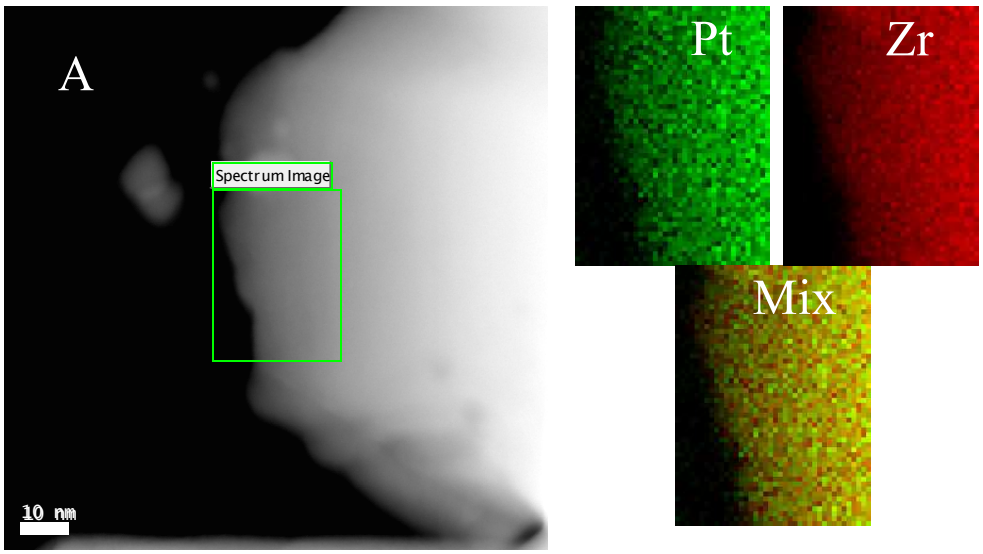

B

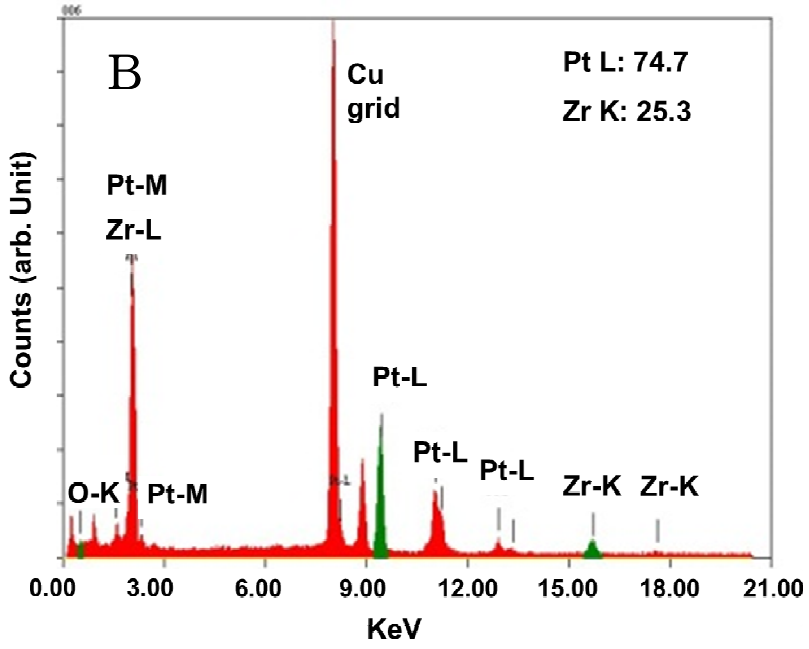

Figure S5. A) STEM image of *h*-$ZrPt_3$ NPs and the corresponding compositional-mapping images. B) The result of compositional analysis is presented.

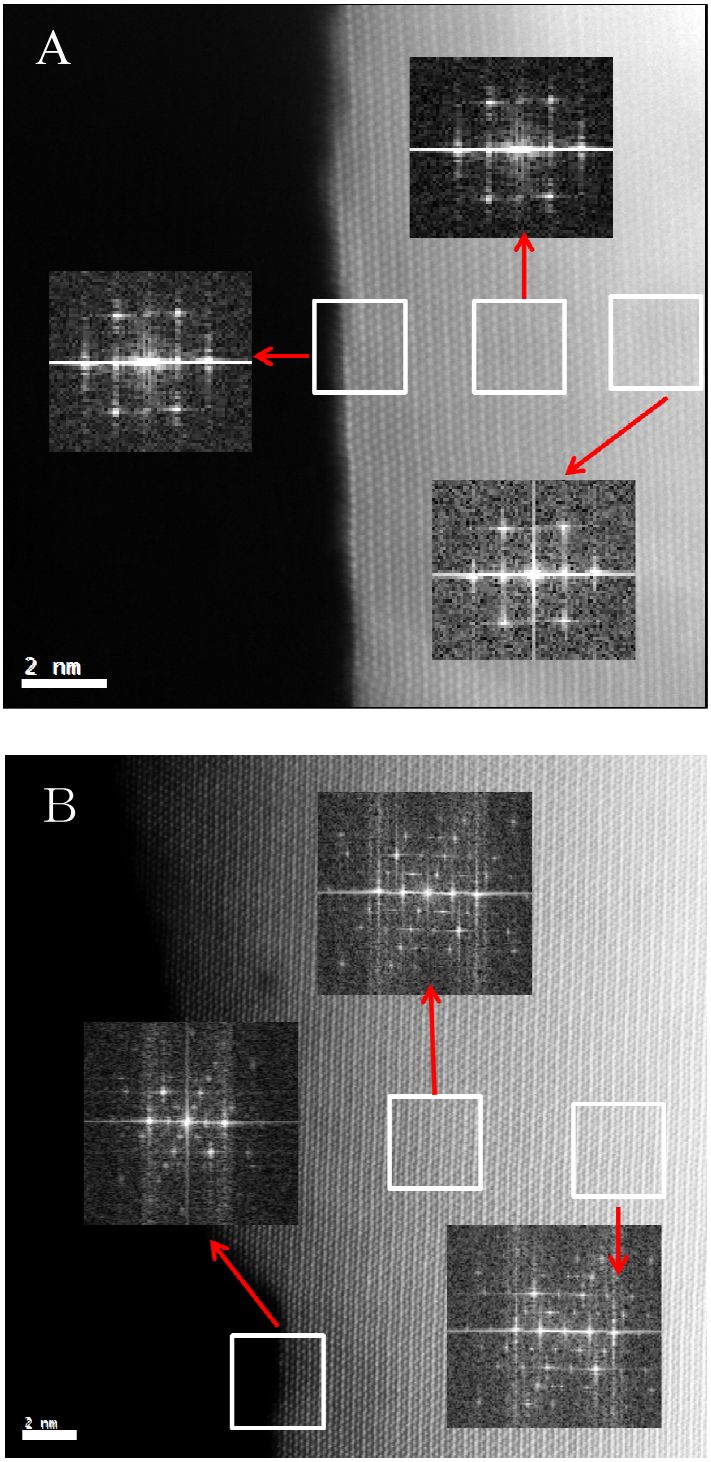

Figure S6. Atomic-resolution STEM images of the A) *c*-$ZrPt_3$ NPs and B) *h*-$ZrPt_3$ NPs. The insets show Fast-Fourier Transform (FFT) patterns, corresponding to the area depicted as white rectangles in the STEM images. Note that the FFT patterns calculated at different areas are identical in the arrangement of the reflection spots.

4 Electrochemistry

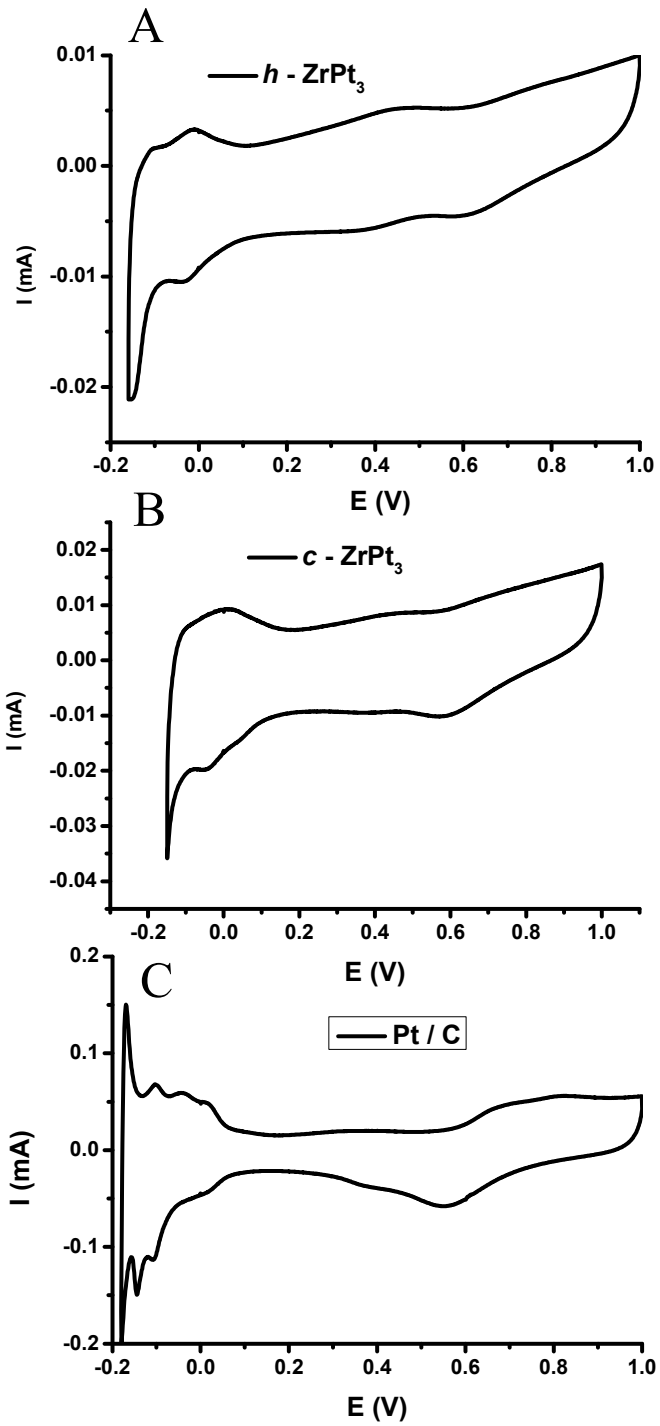

Figure S7. CV profiles of the A) *h*-$ZrPt_3$, B) *c*-$ZrPt_3$ and C) Pt / C in 0.5 M sulfuric acid. Scan rate = 10 mV/sec.

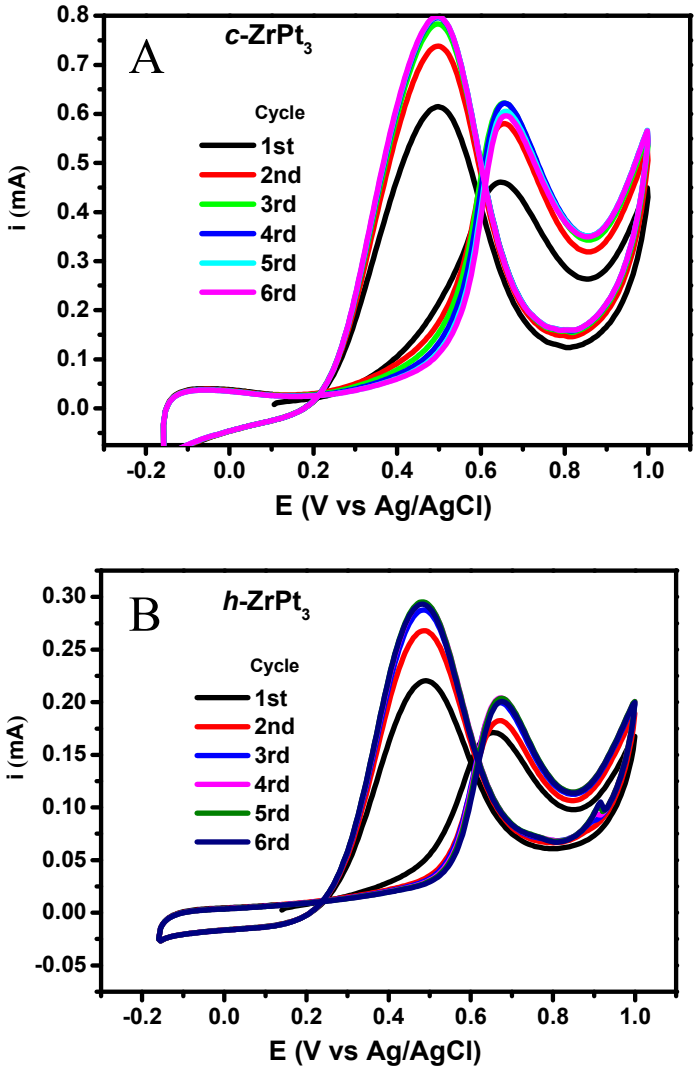

Figure S8. The ethanol-electrooxidation (EOR) currents over the A) *c*-$ZrPt_3$ and B) *h*-$ZrPt_3$ NPs at the early stage of the repeated potential cycles (1^{st} through the 6rd cycles). Acquired in 0.5 M sulfuric acid solution containing 1 M ethanol. Scan rate = 50 mV/sec.

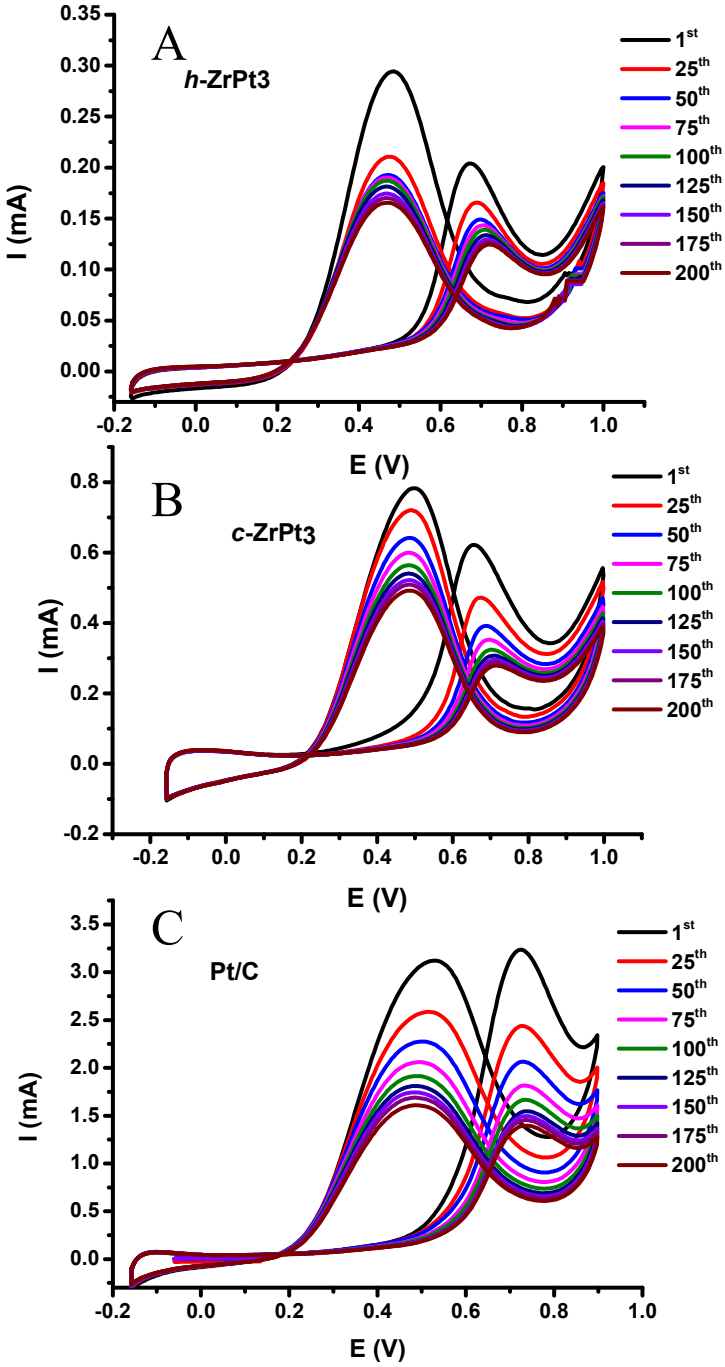

Figure S9. Change of peak current with increasing cycle number for ethanol oxidation of the A) *h*-$ZrPt_3$, B) *c*-$ZrPt_3$ and C) Pt / C in 0.5 M sulfuric acid containing 1 M ethanol. Scan rate = 50 mV/sec.

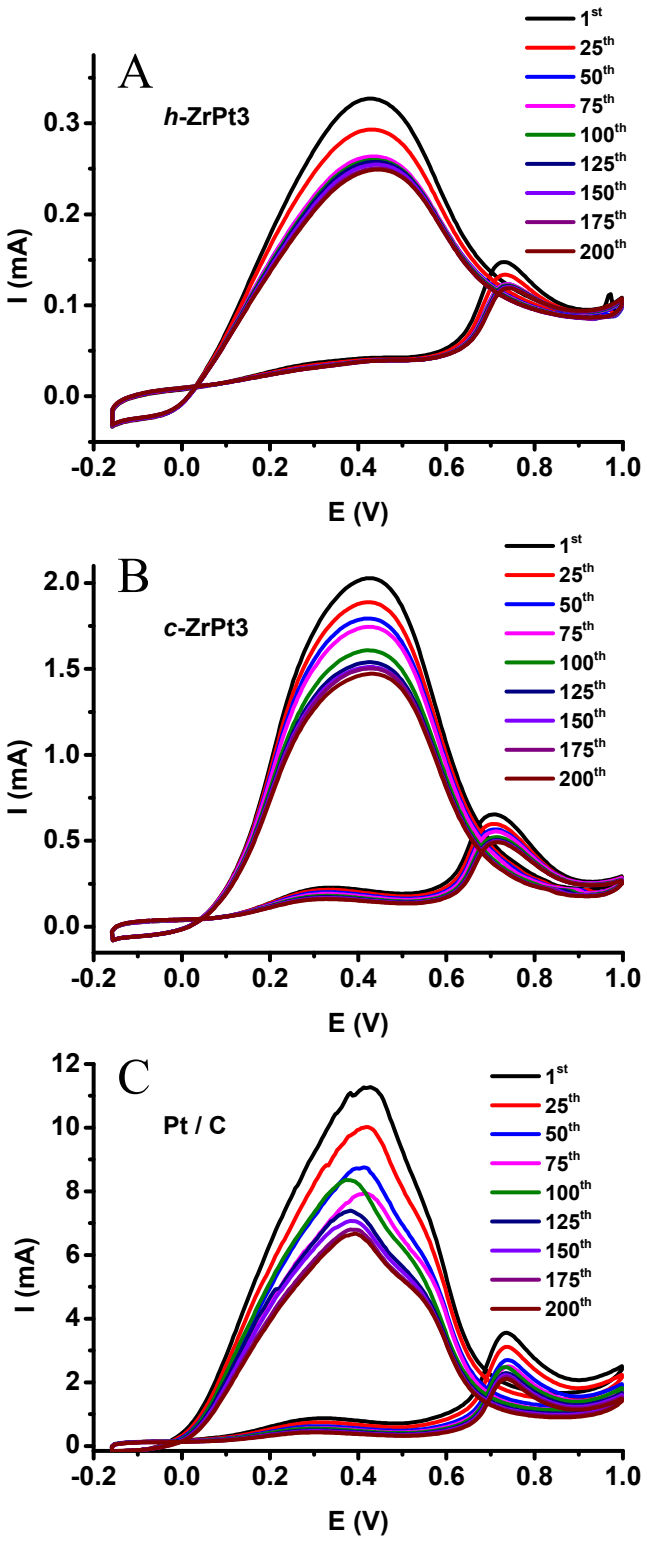

Figure S10. Change of peak current with increasing cycle number for formic acid oxidation of the A) *h*-$ZrPt_3$, B) *c*-$ZrPt_3$ and C) Pt / C in 0.5 M sulfuric acid containing 1 M ethanol. Scan rate = 50 mV/sec.

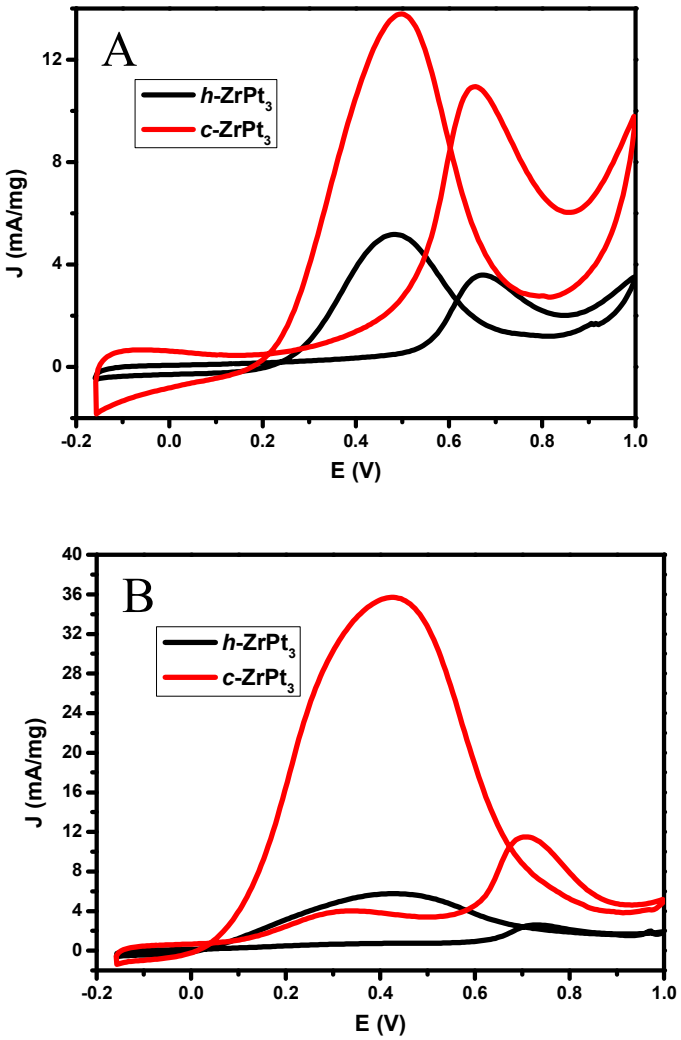

Figure S11. The A) ethanol-electrooxidation (EOR) currents and the B) electrooxidation current for formic acid over the *h*-$ZrPt_3$ and *c*-$ZrPt_3$ NPs, normalized to the loading weight of the catalysts on the electrode (mass activity). Scan rate = 50 mV/sec.

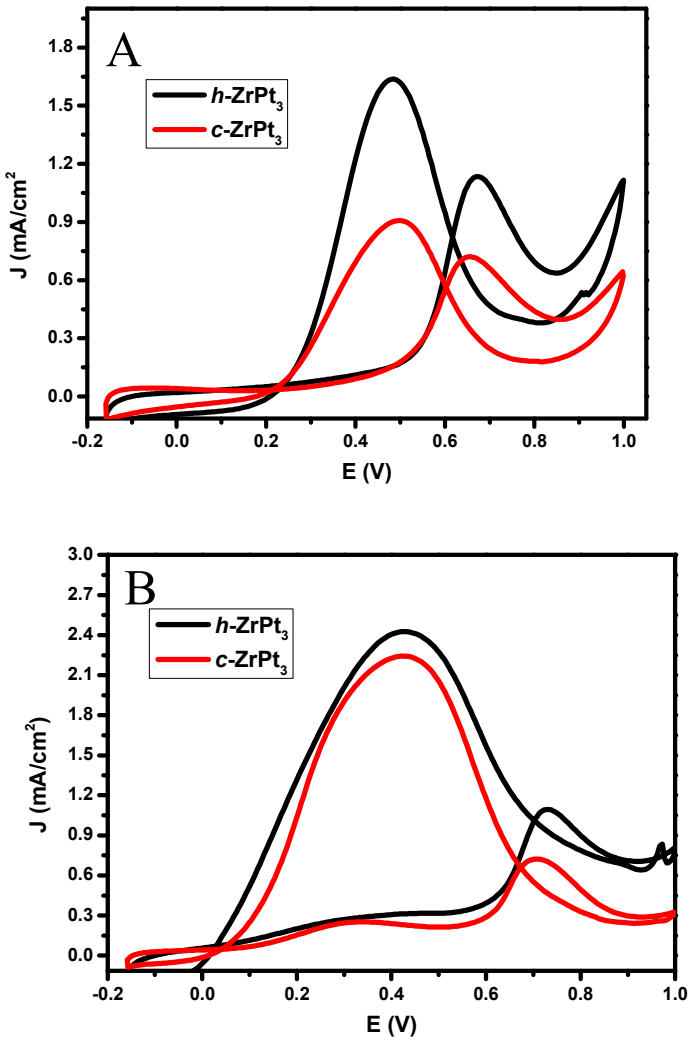

Figure S12. The A) ethanol-electrooxidation (EOR) current and the B) electrooxidation current for formic acid over the *h*-$ZrPt_3$ and *c*-$ZrPt_3$ NPs, normalized to the electrochemical surface area determined from CO stripping experiments. Scan rate = 50 mV/sec.